Research Article | Vol. 29, No. 17 / 16 Aug 2021 / Optics Express 27434
Optics EXPRESS

Soliton based $\chi^{(2)}$ combs in high-Q optical microresonators

S. Smirnov,[1] V. Andryushkov,[1] E. Podivilov,[2] B. Sturman,[2] and I. Breunig[3,4,*]

[1]Novosibirsk State University, 630090 Novosibirsk, Russia
[2]Institute of Automation and Electrometry, Russian Academy of Sciences, 630090 Novosibirsk, Russia
[3]University of Freiburg, Department of Microsystems Engineering - IMTEK, Georges-Köhler-Allee 102, 79110 Freiburg, Germany
[4]Fraunhofer Institute for Physical Techniques IPM, Georges-Köhler-Allee 301, 79110 Freiburg, Germany
*optsys@ipm.fraunhofer.de

Abstract: Investigations of the frequency combs in $\chi^{(3)}$ microresonators have passed a critical point when the soliton based regimes are well established and realized on different platforms. For $\chi^{(2)}$ microresonators, where the first harmonic (FH) and second harmonic (SH) envelopes are coupled via the SH generation and optical parametric oscillation, the comb-soliton studies are just starting. Here we report on a vast accessible dual $\chi^{(2)}$ soliton-comb family in high-Q microresonators with the SH and FH combs centered at the pump frequency ω_p and its half $\omega_p/2$. Vicinity of the point of equal FH and SH group velocities λ_c, available via proper radial poling, is found to be the most advantageous for the generation of spectrally broad dual FH-SH combs. Our predictions as applied to lithium niobate resonators include the dependence of comb and dissipative soliton parameters on the pump power, the deviation $\lambda_p - \lambda_c$, the modal quality factors and frequency detunings, and the necessary parameters of radial poling of the resonator. These predictions form a solid basis for the realization of $\chi^{(2)}$ frequency combs.

1. Introduction

Generation of frequency combs – long sequences of equidistant coherent optical lines – represents nowadays a prosperous scientific area, especially with regard to high-Q optical microresonators [1–8]. Its common feature is search for nonlinear regimes providing and optimizing the necessary comb properties. Compactness, robustness, and strong enhancement of light fields owing to recirculation inside the resonator are highly beneficial for the achievement of the goals. Until recently, the main efforts, both experimental and theoretical, were focused on $\chi^{(3)}$ microresonators and, correspondingly, on Kerr-nonlinearity-controlled comb regimes. The main achievements here are (*i*) realization of identity between high-quality combs and temporal solitons and (*ii*) implementation of this soliton concept into prototypes of real devices. The dissipative solitons in question are fundamentally different from the so-called conservative Kerr solitons. They balance not only the dispersion broadening and nonlinear compression of light envelopes, but also the external pumping and internal losses [4,8,9].

Transfer of the soliton-comb concept to the case of dominating lower-order $\chi^{(2)}$ nonlinearity, employing the processes of second harmonic generation and optical parametric oscillation, represents a big scientific challenge. On the one hand, it promises substantial lowering of pump powers and realization of dual combs centered simultaneously at the first and second harmonics (FH and SH), see also Fig. 1. On the other hand, it forces researches to enter a new area of nonlinear science where many new problems need to be solved. Among these problems is the necessity to fulfill the phase-matching (PM) conditions in microresonators, to deal with both FH and SH dispersions, to account for the temporal walk-off between FH and SH and two frequency detunings, and, finally, to discover new dissipative FH-SH solitons. Phase-matching techniques

#432529 https://doi.org/10.1364/OE.432529
Journal © 2021 Received 8 Jun 2021; revised 28 Jul 2021; accepted 29 Jul 2021; published 10 Aug 2021

Optics EXPRESS

applied in microresonators are birefringent phase-matching [10] and quasi phase-matching [11,12]. The number of material and experimental parameters controlling the nonlinear regimes becomes large compared to the $\chi^{(3)}$ case.

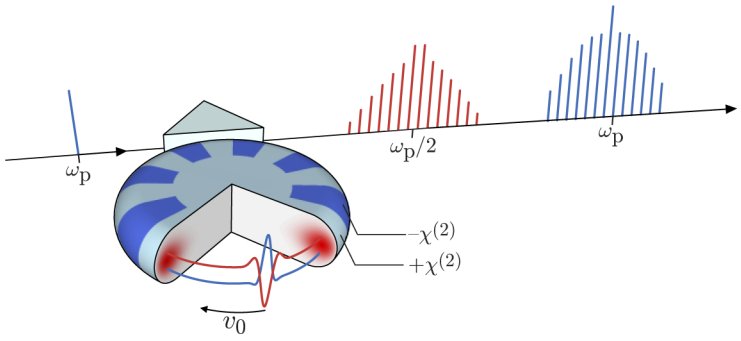

Fig. 1. Principle scheme of soliton-comb generation in $\chi^{(2)}$ microresonators. Monochromatic pump at the frequency ω_p generates dual FH-SH comb owing to quadratic nonlinear processes. It corresponds to FH and SH solitons moving along the resonator rim with a common velocity v_0. Red spots show localization of the resonator modes at the rim, φ is the azimuth angle. A periodic alternation of the sign of $\chi^{(2)}$ coefficients, shown for the number of periods $N = 8$, allows for quasi-PM at an arbitrary frequency ω_p.

A few reviews on the $\chi^{(2)}$ phenomena [13–16] and a number of recent original papers [17–33] serve here as the basis. As $\chi^{(2)}$ microresonators possess also the Kerr response, certain requirements have to be fulfilled to ensure the dominance of quadratic nonlinearity. Sufficienlly large values of the quality factors, $Q \gtrsim 10^7$, were found necessary to neglect the Kerr nonlinearity [16,23,27,32]. This requirement is usually fulfilled for mm-sized $\chi^{(2)}$ resonators. For lower Q-factors typical of on-chip resonators an interplay between $\chi^{(2)}$ and $\chi^{(3)}$ nonlinear processes occurs. Impressive soliton-based combs discovered recently in AlN on-chip resonators [33] are due to this interplay. While experiments [29–31] with high-Q resonators, relevant to large temporal walk-off, show the presence of several comb lines, no evidences of true soliton-based $\chi^{(2)}$ combs are reported so far.

On the theoretical side, coupled equations for the FH and SH light field envelopes $F(\varphi, t)$ and $S(\varphi, t)$ [φ is the azimuth angle] involving the necessary linear and nonlinear terms are known [13,21,22,26–28]. While the SH amplitude S is always 2π-periodic in φ, the FH amplitude F is either periodic or antiperiodic [26–28]. This seemingly surprizing circumstance is fully compatible with periodicity of true light fields inside the resonator [34]. Topologically different periodic and antiperiodic nonlinear solutions correspond to the SH pumping into modes of the resonator with even or odd azimuth numbers, see also Fig. 1. This additional degree of freedom, inherent in $\chi^{(2)}$ resonators, opens new prospects for the frequency combs. In particular, it has been found numerically for the zero detuning case and equal FH-SH decay constants that the excitation of the antiperiodic states leads to the formation of strongly localized stable solitons relevant to spectrally broad dual FH-SH combs [27]. This excitation tends to be especially efficient when approaching the spectral point of zero walk-off where the FH and SH group velocities are equal to each other. It was also predicted that locally stable periodic soliton states can exist at nonzero detunings exactly at the zero walk-off point [21–23]. A few analytical soliton-comb solutions at nonzero FH and SH detunings were found in the limit of small modal decay constants [26,28]; stability of these solutions is questionable. Anyhow, the known theoretical results cover only a tiny part of the perspective regions of experimental and material parameters.

The purpose of this study is to provide a basis of theoretical predictions for realization of net dual frequency-broad soliton-based $\chi^{(2)}$ combs in the vicinity of zero walk-off point. Specifically,

Optics EXPRESS

we consider the case of lithium niobate (LN) based microresonators. This allows us to quantify the wavelength dependences of the dispersion and walk-off parameters and, correspondingly, to narrow the degree of experimental uncertainty. The main variable parameters are the pump power, the spectral distance to the zero walk-off point, the modal FH and SH decay constants (Q-factors) within the actual range, and also small FH and SH frequency detunings relevant to slightly imperfect PM and slightly non-resonant SH pumping. The main predictions are relevant to the number of comb lines, to the soliton localization and velocity, and also to possible bifurcations between different nonlinear regimes. While our specific predictions are relevant to the excitation of the self-starting antiperiodic states, considerable efforts were spent to detect similar periodic states. No such states were found.

The novelty of our study is in a strong development and practical implementation of [27]. We have proceeded from a special single-soliton case to the vast accessible soliton-comb family depending on the pump power parameter, pump wavelength, FH-SH frequency detunings, and quality factors. This family and the scale of predictions have no analogs in the literature.

2. Theoretical background

A $\chi^{(2)}$ microresonator can be conventionally viewed as a ring waveguide of radius R, where the light wavevectors acquire discrete values $k_m = m/R$ with m being the modal azimuth number. The modal frequency is expressed by m as $\omega_m = mc/Rn$, where c is speed of light and n is the refractive index. Slow dependence of n on the vacuum wavelength λ includes generally the bulk part and geometrical corrections [35–37]. Usually, $R \sim 1$ mm for LN based resonators and, correspondingly, $m \sim 10^4$ for the optical range. The geometric corrections to n are negligible here, and the dependence $n(\lambda)$ is well known for LN crystals [38–40]. Radial poling corresponds to a φ-periodic alternation of the direction of the spontaneous polarization, see also Fig. 1. It does not influence the linear optical properties, but changes the sign of the major $\chi^{(2)}$ coefficients. By choosing properly the number of poling periods $\mathcal{N}$ and using the fine-tuning means [41–43], one can adjust PM practically to any desirable pump wavelength λ_p without substantial weakening of the efficient nonlinear coefficient [11,37]. The birefringent PM does not require structuring of the resonator, but it attaches one to a very narrow range of λ_p ($\lambda_p \simeq 0.532$ μm for LN [10]). The experimental comb studies [29–33] employed the natural PM.

Importantly, the quasi-PM conditions $m_p - \mathcal{N} = 2m_1$, $\omega_{m_p} = 2\omega_{m_1}$, where m_1 is a FH azimuth mumber, can be fulfilled only for even $m_p - \mathcal{N}$. For odd $m_p - \mathcal{N}$, we must use instead $m_p - \mathcal{N} = 2m_1 + 1$, $\omega_{m_p} = \omega_{m_1} + \omega_{m_1+1}$ leading to the parametric excitation of two FH modes. These two cases correspond to the topologically different periodic (P) and antiperiodic (A) light states [26,27].

Coupled nonlinear equations describing the temporal evolution of the FH and SH complex light envelopes $F(\varphi, t)$ and $S(\varphi, t)$ owing to the $\chi^{(2)}$ nonlinearity have the following generic form [26,27]:

$$\begin{aligned}\left[\mathrm{i}\left(\frac{\partial}{\partial t} + \frac{v_1}{R}\frac{\partial}{\partial \varphi} + \gamma_1\right) + \frac{v_1'}{2R^2}\frac{\partial^2}{\partial \varphi^2} - \Delta_1\right]F &= 2\mu S F^* \\ \left[\mathrm{i}\left(\frac{\partial}{\partial t} + \frac{v_2}{R}\frac{\partial}{\partial \varphi} + \gamma_2\right) + \frac{v_2'}{2R^2}\frac{\partial^2}{\partial \varphi^2} - \Delta_2\right]S &= \mu F^2 + \mathrm{i}h.\end{aligned} \tag{1}$$

The subscripts 1 and 2 refer to the FH and SH parameters, respectively, $v_{1,2}$ and $v_{1,2}'$ are the group velocities and the dispersions (discrete equivalents of $d\omega/dk$ and $d^2\omega/dk^2$), $\gamma_{1,2}$ are the modal decay constants linked to the quality factors as $Q_{1,2} = \omega_{1,2}/2\gamma_{1,2}$, $\Delta_1 = (2\omega_{m_1} - \omega_p)/2$ and $\Delta_2 = \omega_{m_p} - \omega_p$ are the frequency detunings accounting for slightly imperfect PM and resonance with mode m_p, μ is the efficient coupling coefficient, and h is the efficient pump strength. All introduced parameters are real and experimentally controlled; the ratios $v_{1,2}/2\pi R$ ($\gtrsim 10$ GHz) are known as FH and SH free spectral ranges. The amplitudes F and S can refer to different

Optics EXPRESS

or the same light polarizations. The largest coupling coefficient corresponds to the case of the same extraordinary polarization [40], which is beneficial for the radial poling. Dependences $v_{1,2}(\lambda_p)$ and $v'_{1,2}(\lambda_p)$ for lithium niobate (and the extraordinary polarization) are shown in Fig. 2. The point $\lambda_c \simeq 1.349\ \mu$m corresponds to zero walk-off, $v_{12} \equiv v_1 - v_2 = 0$. In the vicinity of this point we have v_{12}[cm/s] $\simeq -5.9 \times 10^5\ \delta\lambda$ [nm], $v'_1 \simeq 0.8$, and $v'_2 \simeq -0.4$ of 10^4 cm^2/s, where $\delta\lambda = \lambda_p - \lambda_c$.

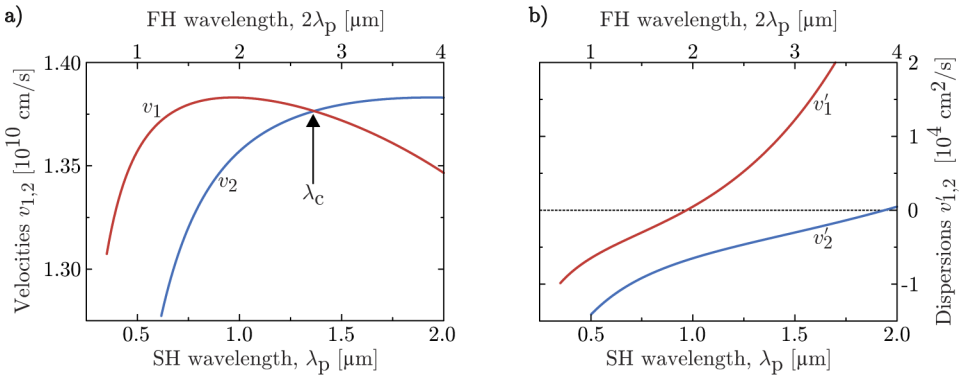

Fig. 2. Wavelength dependences of the group velocities $v_{1,2}$ (a) and dispersions $v'_{1,2}$ (b) for LN resonators at the extraordinary polarization and room temperature. For the radius $R \gtrsim 1$ mm the geometric corrections are negligible with a high accuracy. The arrow in a) indicates the point of equal velocities $\lambda_c \simeq 1.349\ \mu$m.

Set (1) is relevant to the both P and A light states. These states are different in symmetry. For the P- and A-cases, the FH amplitude obeys the circumvention conditions $F(\varphi, t) = F(\varphi + 2\pi, t)$ and $F(\varphi, t) = -F(\varphi + 2\pi, t)$, respectively. The circumvention condition for the SH amplitude $S(\varphi, t)$ is always 2π-periodic. However, because of the nonlinear coupling with F, the amplitude S is substantially different for the P- and A-cases. Temporal evolution can never break the symmetry of solution.

Set (1) possesses spatially uniform steady-state solutions $\bar{F}$, $\bar{S}$, as quantified in Appendix A. These solutions form backgrounds for localized FH-SH solitons. Remarkably, the background $\bar{F}$ is determined up to the sign. For the P- and A-solitons the left and right FH backgrounds must thus be the same and opposite, respectively. Spatio-temporal stability of the FH-SH background is necessary for the existence of stable dual FH-SH solitons.

Fourier expansions for the envelopes,

$$S = \sum_l S_l \exp(\mathrm{i}l\varphi), \quad F = \sum_j F_j \exp(\mathrm{i}j\varphi)\ , \tag{2}$$

where $S_l = S_l(t)$ and $F_j = F_j(t)$, are useful. For both P- and A-cases the number l takes values $0, \pm1, \pm2, \ldots$. The number j takes the same integer values in the P-case, but semi-integers $\pm1/2, \pm3/2, \ldots$ in the A-case. The Fourier harmonics F_0, S_0 should not be mixed up with the backgrounds $\bar{F}, \bar{S}$. In particular, $F_0 = 0$ for A-solitons can coexist with opposite left-right backgrounds $\pm\bar{F}$ far from the soliton center. Using Eq. (2), set (1) can be transformed to an equivalent set of ordinary differential equations for F_j and S_l, see Appendix B for details.

The comb generation is due to the parametric instability of the spatially uniform trivial solution $S_0 = h/(\gamma_2 + \mathrm{i}\Delta_2)$, $F_0 = 0$ against small perturbations. Only harmonics F_j and F^*_{-j} are coupled with each other within the linear approximation. This yields an expression for the instability threshold

$$4\mu^2 h_{\mathrm{th}}^2 = [\gamma_1^2 + (\Delta_1 + j^2 v'_1/2R^2)^2](\gamma_2^2 + \Delta_2^2) \tag{3}$$

Optics EXPRESS

that depends on j^2 and FH dispersion v_1', but does not depend on v_2' and $v_{1,2}$. Also, it is not symmetric in Δ_1 and Δ_2. The threshold value of $|S_0|^2$ corresponding to Eq. (3) is $|S_0|^2_{\text{th}} = |h|^2_{\text{th}}/(\gamma_2^2 + \Delta_2^2)$, it also depends on j^2. The minimum in $\Delta_{1,2}$ value of h^2_{th} is $(\gamma_1\gamma_2/2\mu)^2$; it does not depend on j^2 and corresponds to $\Delta_1 = -j^2 v_1'/2R^2$ and $\Delta_2 = 0$, when the dispersion shift of the modal frequency is compensated and the mode m_p is pumped resonantly. At this minimum we have $|S_0|_{\text{th}} = \gamma_1/2\mu$. For $h>h_{\text{th}}$, the quantities F_j and F^*_{-j} grow exponentially in time within the linear approximation and oscillate as $\exp(-\mathrm{i}jv_1 t/R)$. This means that the FH light pattern moves along the rim with velocity v_1. This analysis is applicable both to the P- and A-cases.

We can consider steady-state light patterns $F(\varphi, t)$ and $S(\varphi, t)$ above the threshold as a result of nonlinear saturation of the initial exponential growth of small perturbations. We are especially interested in strongly localized steady-state FH and SH light patterns propagating with the same velocity v_0: $F = F(\varphi - v_0 t/R)$, $S = S(\varphi - v_0 t/R)$, i.e. in dual FH-SH solitons. Establishment of such states is not granted but highly desirable for $\chi^{(2)}$ combs. Fourier expansions (1) of such states lead automatically to equidistant lines with the same spacing v_0/R within the FH and SH frequency domains, i.e. to the dual frequency comb. The spectral width of this comb is inversely proportional to the soliton localization scale. As the emerging FH modes propagate with velocity v_1 at the threshold, one can suggest that $v_0 \simeq v_1$ for sufficiently small super-criticalities. The velocity difference $v_{01} = v_0 - v_1$ is a crucial soliton parameter. It has to be determined simultaneously with shape of the FH and SH envelopes and be dependend on the pump strength h and other variable parameters. What can be alternatives to such steady-state patterns? It can be light states corresponding to a few or several localized solitons. It can also be chaotic saturated states. It seems all alternatives are not beneficial for the combs.

The basic set (1) refers to a static coordinate frame. As we expect that steady-state light patterns propagate with velocity $v_0 \simeq v_1$, it is practical to rewrite it for a coordinate frame moving with velocity v_1. To do this, it is sufficient to drop the term $v_1\partial_\varphi$ in the first equation and replace v_2 by $-v_{12} = v_2 - v_1$ in the second equation. Harmonics $F_j(t)$ and $S_l(t)$ calculated in this moving frame oscillate as $\exp(-\mathrm{i}jv_{01}t/R)$ and $\exp(-\mathrm{i}lv_{01}t/R)$ for steady-state light patterns propagating with velocity v_0. When applied to numerical data, this general oscillation law enables one (*i*) to make sure that we deal with a desirable steady state and (*ii*) to evaluate $v_{01} = v_0 - v_1$ with a high accuracy. Details of the calculation procedure can be found in [27], see also Sect. 3. In essence, the velocity difference v_{01} is a measure of the FH-SH coupling strength. Furthermore, the ratio v_{01}/R gives correction to the frequency spacing v_1/R between the comb lines. Dependence of v_{01} on the variable parameters, see below, means comb tunability.

Lastly, we discuss shortly the most important variable parameters of our nonlinear system: h, λ_p, $\gamma_{1,2}$, and $\Delta_{1,2}$; totally six real parameters.

– The squared pump strength h^2 is proportional to the pump power $\mathcal{P}$, so the super-criticality parameter $\eta = h/h^{\text{min}}_{\text{th}} = 2\mu h/\gamma_1\gamma_2 = (\mathcal{P}/\mathcal{P}^{\text{min}}_{\text{th}})^{1/2}$. It can be regarded as a useful experimental parameter.

– The choice of the pump wavelength λ_p (implying the radial poling) is crucial for $\chi^{(2)}$ combs. On the one hand, it predetermines the number of radial poling periods that cannot be changed afterwards. On the other hand, it affects the nonlinear regimes and comb properties. The point is that the velocity difference $v_{12} = v_1 - v_2$ varies from zero at $\lambda_c \simeq 1.349\ \mu$m to very large values ($\sim \pm 10^9$ cm/s) for $|\lambda_p - \lambda_c| \gtrsim 0.5\ \mu$m. For so high values of $|v_{12}|$, the term $v_{12}l/R$ in the left-hand side of equations for S_l with $l \neq 0$ is dominating for any reasonable choice of R and γ_2. This suppresses harmonics S_l and the related nonlinear processes. Thus, vicinity of the point λ_c is the most beneficial for $\chi^{(2)}$ combs.

– Large quality factors $Q_{1,2} = \omega_{1,2}/2\gamma_{1,2}$ typical of LN based resonators are also beneficial for the combs. Usually, $Q_{1,2} \lesssim 10^8$ [15,16]. To cover the actual ranges of $Q_{1,2}$, we varied $\gamma_{1,2}$ independently from 10^7 to 10^8 s^{-1}.

Optics EXPRESS

– The frequency detunings $\Delta_{1,2}$ were varied independently within intervals sufficient to resolve the major features of the comb behavior.

When representing the FH and SH soliton intensities $|F(\varphi)|^2$ and $|S(\varphi)|^2$ and also the FH and SH comb spectra $|F_j|^2$ and $|S_l|^2$, we normalize them to $\gamma_1\gamma_2/2\mu^2$ and $\gamma_1^2/4\mu^2$, respectively. This normalization does not include $\Delta_{1,2}$; for $\gamma_1 = \gamma_2$ it corresponds to [27].

3. Numerical methods

We simulated numerically set (6) for the Fourier harmonics $F_j(t)$ and $S_l(t)$ as applied to the P- and A-cases using the fourth-order Runge-Kutta method in vicinity of zero walk-off point λ_c and within sufficiently broad ranges of $\eta = h/h_{\rm th}^{\rm min}$, $\gamma_{1,2}$, and $\Delta_{1,2}$. Our λ_p-mesh explicitly included the zero walk-off point λ_c. The number of harmonics within each of the FH and SH frequency domains ranged from 32 to 1024. The calculation accuracy was controlled via changing the time step and the total number of harmonics.

With the Fourier harmonics $F_j(t)$, $S_l(t)$ calculated, we were able to make sure that steady-state light patterns are established and to calculate the velocity difference $v_{01} = v_0 - v_1$, the comb spectra $|F_j|^2$ and $|S_l|^2$, and the spatial (soliton) profiles $F(\varphi)$ and $S(\varphi)$ in the coordinate frame moving with velocity v_0. The relevant numerical correlation procedure for F (and analogously for S) was as follows: Using the relations of Sect. 2 for the Fourier harmonics, we calculated the quantity $\varepsilon = \sum_j |F_j(t) - F_j(t+\tau)|^2 / \sum_j (|F_j(t)|^2 + |F_j(t+\tau)|^2)$ in a coordinate frame moving with a probe velocity $\tilde{v}_0$. For sufficiently large time t and the time shift τ, ε tends rapidly to zero if and only if a steady state is achieved and $\tilde{v}_0 = v_0$. This has enabled us to calculate v_0 with a relative accuracy better than 10^{-5}. Further details can be found in [27].

An adiabatic calculation procedure was widely used: At the first step, we set h slightly above $h_{\rm th}$ and employed very small random amplitudes as initial conditions. After that, the pump strength h increased stepwise, and the values of $F_j(t_s)$ and $S_l(t_s)$ achieved at time t_s and relevant to steady-state values of $|F_j(t_s)|$ and $|S_l(t_s)|$ were used as new initial data for the next calculation run with larger or smaller values of h. Establishment of the intermediate steady states was controlled with a high accuracy. A similar adiabatic procedure was used to investigate the effects of the frequency detunings $\Delta_{1,2}$.

4. Results: Zero-detuning case

We start from a demonstration of the properties of the steady-state solutions relevant to the case of zero detunings $\Delta_{1,2} = 0$, the super-criticality parameter $\eta = h/h_{\rm th} = 30$, and decay constants $\gamma_1 = 10^7$, $\gamma_2 = 10^8$ s^{-1} corresponding to $Q_1 \simeq 3.5\times10^7$, $Q_2 \simeq 0.7\times10^7$. Also two representative values of the spectral parameter $\delta\lambda = \lambda_p - \lambda_c$ are considered. Both periodic and antiperiodic solutions were tried within our adiabatic procedure. While in the A-case, similarly to [27], we robustly arrived to single-soliton solutions different only in position in the cavity, in the P-case we got no single-soliton solution. Instead, we observed typically dual steady-state background solution $\bar{F}, \bar{S}$. This correlates with the results of [23] on realization of periodic soliton solutions under special conditions and $\Delta_{1,2} \neq 0$. Thus, the periodic solitons seem to be rather special as compared to the antiperiodic ones. This is why we focus on the A-case.

Figures 3(a) and 3(b) show in some detail the normalized steady-state FH and SH intensity profiles $|F(\varphi)|^2$ and $|S(\varphi)|^2$ for the zero walk-off point $\delta\lambda = \lambda_p - \lambda_c = 0$. We have a well localized dark-bright FH-SH soliton moving with velocity $v_0 = v_1 = v_2$. Both profiles are symmetric with regard the replacement $\varphi \leftrightarrow -\varphi$ and possess backgrounds. In accordance with Appendix A, the FH and SH background values are $\eta - 1 = 29$ and 1, respectively. Remarkably, the minimum value of $|F(\varphi)|^2$ is zero and the maximum normalized value of $|S(\varphi)|^2$ is very large $\simeq 613$. The function $\arg[F(\varphi)]$, not shown in Fig. 3, varies by π across the the resonator; this is the general property of the antiperiodic states [26,27].

Optics EXPRESS

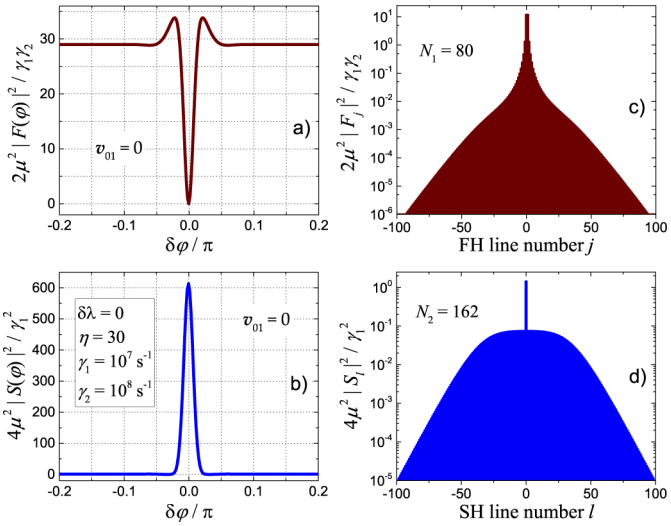

Fig. 3. Zero walk-off point, $\delta\lambda = 0$: Representative dual FH and SH soliton profiles (a,b) and comb spectra (c,d) for $\eta = 30$, $\gamma_1 = 10^7$ and $\gamma_2 = 10^8$ s^{-1}. The azimuth angle variation $\delta\varphi$ is counted from the soliton center. The insets give the values of the velocity difference $v_{01} = v_0 - v_1$ and the comb line numbers N_1 and N_2 relevant to the FH and SH comb spectra. The total comb line number is $N = N_1 + N_2$.

Figures 3(c) and 3(d) exhibit the corresponding FH and SH comb spectra $2\mu^2|F_j|^2/\gamma_1\gamma_2$ and $4\mu^2|S_l|^2/\gamma_1^2$ consisting of equidistant lines with the frequency spacing v_0/R. They both are symmetric in j and l, respectively. The shapes of the FH and SH spectra are substantially different. It is remarkable also that the maximum values $2\mu^2|F_{\pm1/2}|^2/\gamma_1\gamma_2$ are pretty large ($\simeq 12$). The maximum value $4\mu^2|S_0|^2/\gamma_1^2$ is close to 1, and it substantially exceeds the side values. This means that the harmonic S_0 stays close to the threshold while all other harmonics are deeply below the threshold.

As a simple and useful measure of the FH and SH comb widths, here and later we employ parameters N_1 and N_2 – the numbers of lines in the spectra $|F_j|^2$ and $|S_l|^2$ exceeding 10^{-4} of $|F_j|^2_{\max}$ and $|S_l|^2_{\max}$, respectively. Then the total number of comb lines is $N = N_1 + N_2$. Our definition of $N_{1,2}$ does not depend on the normalization procedure. For the Figs. 3(c) and 3(d) we have $N_1 = 80$, $N_2 = 162$, and $N = 242$. Note that our estimate of N_1 is somewhat undervalued: Since $|F_j|^2_{\max} \gg |S_l|^2_{\max}$, the number of FH comb lines exceeding some reasonable noise level can be notably larger than N_1.

Now we turn to the case $\delta\lambda \neq 0$. Figures 4(a) and 4(b) show the normalized soliton profiles for $\delta\lambda \simeq -1.08$ nm and the same other parameters. The relative soliton velocity v_{01} is non-zero here and equal to $\simeq 6 \times 10^5$ cm/s, which is slightly below $v_{12}(\delta\lambda) \simeq 6.4 \times 10^5$ cm/s. Velocity v_0 lies thus outside the interval $[v_1, v_2]$. The profiles $|F(\varphi)|^2$ and $|S(\varphi)|^2$ lose the $\varphi \leftrightarrow -\varphi$ symmetry, but keep the same background values. The change of the FH profile is especially notable, compare Figs. 3(a) to 4(a): The profile acquires an oscillatory structure and loses the zero point. The relevant FH and SH comb spectra are shown in Figs. 4(c) and 4(d). They are notably asymmetric in j and l, but otherwise carrying the same general features. The comb line numbers $N_{1,2}$ and N are slightly higher than they are in the case $\delta\lambda = 0$. Thus, the condition $v_{12} = 0$ is not necessarily optimal for the comb generation, see also below. Inversion of $\delta\lambda$ changes the sign of v_{01} and transforms all dependences of subfigures a) to d) to the mirror-reflected about the vertical zero-lines. Note that all subsequent soliton profiles and comb spectra are qualitatively similar to those shown in Fig. 3.

Optics EXPRESS

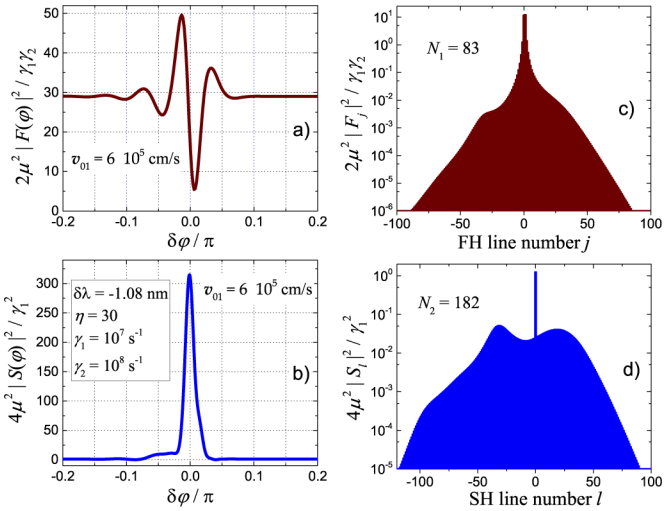

Fig. 4. Nonzero walk-off, $\delta\lambda = -1.08$ nm: FH and SH soliton profiles (a,b) and comb spectra (c,d). The input parameters and explanations are the same as in Fig. 3.

What happens with the soliton-comb parameters when changing $\delta\lambda$, η, and $\gamma_{1,2}$? Calculation of color maps of velocity v_{01} and the comb line number N on the $\delta\lambda, \eta$-plane clarifies the situation. To see the effect of $\gamma_{1,2}$ on these properties, we consider such maps for three combinations of the decay constants, see Fig. 5. Subfigures of the upper row represent the map $v_{01}(\delta\lambda, \eta)$ for $\gamma_{1,2} = \gamma$ (a1), $\gamma_1 = \gamma$, $\gamma_2 = 10\gamma$ (b1), and $\gamma_1 = 10\gamma$, $\gamma_2 = 10\gamma$ (c1), where $\gamma = 10^7$ s^{-1}. Subfigures a2), b2), and c2) give the corresponding maps of the total comb line number N. Subfigures d1) and d2), supplementing the color maps, give representative cross-sections $v_{01}(\delta\lambda)$ and $N(\delta\lambda)$ for $\eta = 20$ relevant to our combinations of $\gamma_{1,2}$.

The most general soliton-comb properties are:

- There are two different regimes – the walk-off regime for sufficiently large values of $|\delta\lambda|$ and the dispersion regime in the close vicinity of $\delta\lambda = 0$.
- The soliton velocity $v_{01}(\delta\lambda, \eta)$ turns to zero at the line $\lambda_p = \lambda_c$; the comb line number N and $|v_{01}|$ experience shallow and deep dips when crossing this line.
- With a good accuracy $v_{01}(\delta\lambda, \eta)$ and $N(\delta\lambda, \eta)$ are odd and even in $\delta\lambda$, respectively.
- Both $|v_{01}|$ (for $\delta\lambda \neq 0$) and N grow monotonously with increasing η. For the walk-off regime, they decrease with increasing spectral distance $|\delta\lambda|$. This decrease persists for $|\delta\lambda|$>10 nm.

Further important and remarkable properties depend on $\gamma_{1,2}$. One sees from Fig. 5 that the maximum in $\delta\lambda$ and η values of $|v_{01}|$ and N grow with increasing both γ_1 and γ_2. It is necessary, however, to take into account that keeping the same value of η with increasing $\gamma_{1,2}$ means increasing pump power in accordance with our definition $\eta = 2\mu h/\gamma_1\gamma_2$. Thus, larger values of $N_{\max}$ in a2), b2), c2) correspond to larger pump powers. On the other hand, this increase can be explained by the balance between the dissipative and dispersion terms in the left-hand sides (LHSs) of Eqs. (1): the larger $\gamma_{1,2}$, the higher values of $|j|$ and $|l|$ are needed to reach this balance.

The spectral width of the dispersion area, which can be defined as the distance between maxima of $|v_{01}|(\delta\lambda)$, also grows with $\gamma_{1,2}$, see, e.g., Fig. 5(d1). This feature can be explained by balancing the walk-off and dissipative contributions in Eqs. (1). The effect of the ratio γ_2/γ_1 is

Optics EXPRESS

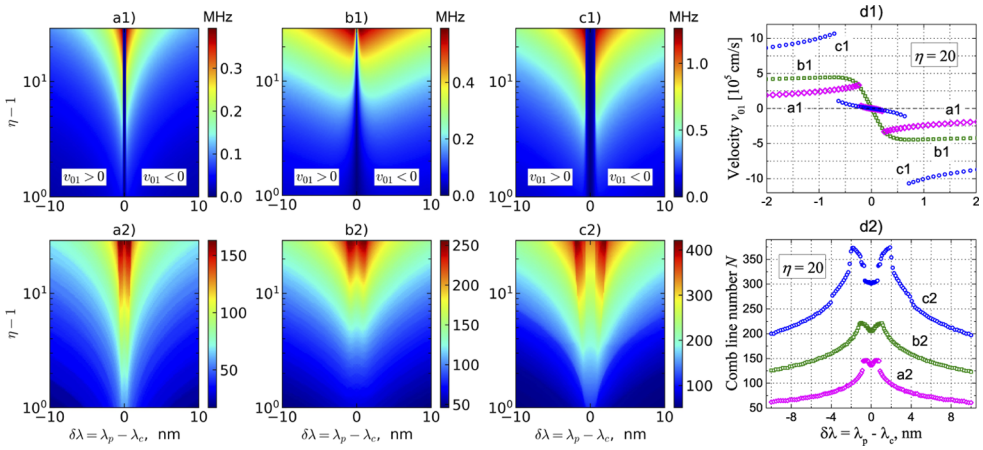

Fig. 5. a1) to d2): Color maps of the velocity parameter $|v_{01}|/2\pi R$ [MHz] (first row) and of the total comb line number $N = N_1 + N_2$ (second row) on the $\delta\lambda, \eta$-plane in steady state. The first, second, and third columns correspond to $\gamma_{1,2} = \gamma$, $\gamma_1 = \gamma$, $\gamma_2 = 10\gamma$, and $\gamma_{1,2} = 10\gamma$, respectively, where $\gamma = 10^7$ s^{-1}. Each map is obtained by stepwise increase of η starting from the value of 2 and incorporates the data of $141 \times 151 = 21291$ calculation variants with up to 1024 Fourier harmonics taken into account. The whole range of $\delta\lambda$ covers about 200 FSRs. The insets in maps a1), b1), and c1) indicate the signs of v_{01}. Subfigures d1) and d2), supplementing the maps, show the crosssections $v_{01}(\delta\lambda)$ and $N(\delta\lambda)$ for $\eta = 20$ relevant to the maps a1) to c1) and a2) to c2), respectively. Note different scales of $\delta\lambda$ in subfigures d1) and d2).

also remarkable. While for $\gamma_2/\gamma_1 = 1$ we have a sharp quasi-discontinuity of $v_{01}(\delta\lambda)$ (see the blue and magenta dotted lines), for $\gamma_2/\gamma_1 = 10$ this discontinuity is smoothed (see the green dotted line in Fig. 5(d1). The points of maxima of $N(\delta\lambda)$ are notably shifted outwards against the points of maxima of $|v_{01}|(\delta\lambda)$. For example, $N(\delta\lambda)$ peaks at $\delta\lambda \simeq \pm 2$ nm for the blue dotted line in Fig. 5(d2), while $|v_{12}|(\delta\lambda)$ has maxima at $\delta\lambda \simeq \pm 0.7$ nm.

In the whole shown range of $\delta\lambda$ and η the soliton velocity v_0 lies outside the interval $[v_1, v_2]$. As concerns the velocity ratio $|v_{01}|/|v_{12}|$, it can exceed 1 only for $|\delta\lambda| \lesssim 1$ nm.

5. Results: effects of $\Delta_{1,2}$

The presence of nonzero frequency detunings $\Delta_{1,2}$ changes the situation quantitatively and, largely, qualitatively. In order to gain insights into the impact of $\Delta_{1,2}$ on the soliton-comb properties, we adiabatically scanned the Δ_1, Δ_2 plane starting from an antiperiodic steady state relevant to $\Delta_{1,2} = 0$. As a representative pump strength parameter we have chosen $\eta = 30$. In fact, two similar scanning procedures were used. Within the first one, we determined initially the soliton velocity v_{01} and the comb line number $N = N_1 + N_2$ by increasing and decreasing Δ_1 at $\Delta_2 = 0$. After that, starting from a point $\Delta_1, 0$, we increased and decreased detuning Δ_2. The achieved steady-state values of the amplitudes F_j and S_l were used as new initial conditions in each step of changing Δ_1 or Δ_2. Within the second procedure, the scanning order was inverted: initially we varied Δ_2 at $\Delta_1 = 0$, and after that increased and decreased Δ_1 starting from points $0, \Delta_2$. We have verified whether the quantities $v_{01}(\Delta_1, \Delta_2)$ and $N(\Delta_1, \Delta_2)$ depend of the scanning order. Also, we have made sure that each steady state on the Δ_1, Δ_2 plane is still relevant to a single-soliton A-state.

Turning to particularities, we consider first what happens strictly at the zero walk-off point $\lambda_p = \lambda_c$, where $v_1 = v_2$. In our coordinate frame moving with velocity v_1, the positive and

Optics EXPRESS

negative propagation directions are equivalent, so that the soliton velocity difference $v_{01} = v_0 - v_1$ is expected to be zero in steady state. This would also be in agreement with Sect. IV. Surprizingly, we have found that this is not always the case.

Consider the map of $|v_{01}|/2\pi R$ for the decay constants $\gamma_1 = 10^7$, $\gamma_2 = 10^8$ s^{-1}, see Fig. 6(a). The uniformly dark-blue colored lower and upper parts, which are separated from the rest by two slanted borders (bifurcation lines), correspond to $v_{01}/2\pi R = 0$ within an accuracy of about 10^{-9} MHz. Between these borders we have a well pronounced distribution $|v_{01}|(\Delta_1, \Delta_2)$ whose scale is comparable with that relevant to Fig. 5. This distribution practically does not depend on the scanning order. But what about the sign of v_{01}? It is found to be quasi-randomly dependent on fine particularities of our numerical calculations, such as the presence of very weak remnant velocity perturbations. In essence, we have a clear example of the spontaneous symmetry breaking, when the state with a high symmetry ($v_{01} = 0$) becomes unstable against the excitation of one of two equivalent states with lower symmetry ($|v_{01}| \neq 0$). The ferroelectric second-order transition below the Curie temperature is perhaps one of the most known examples of such a symmetry breaking. Continuous (without jumps) character of the dependence $|v_{01}|(\Delta_1, \Delta_2)$ near the bifurcation lines, see Fig. 6(a), supports this analogy. Within a very narrow strip near the slanted borders the results of our calculations depend on the scanning order. This is a hysteresis region inherent in second-order phase transitions.

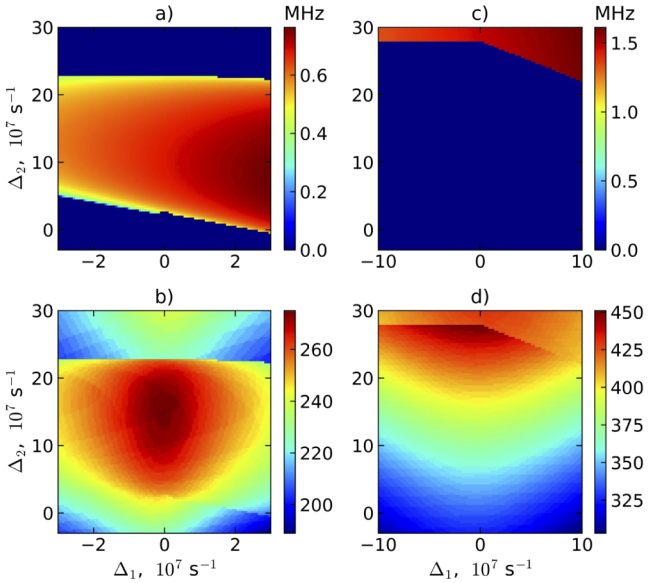

Fig. 6. Zero walk-off point, $\lambda_p = \lambda_c$: Color maps of the soliton velocity parameter $|v_{01}|/2\pi R$ (the upper row) and of the total comb line number $N = N_1 + N_2$ (lower row) on the Δ_1, Δ_2 plane for $\eta = 30$. Each map incorporates the data of $90 \times 90 = 8100$ calculation variants with a constant step in $\Delta_{1,2}$. Maps a) and b) correspond to $\gamma_1 = 10^7$, $\gamma_2 = 10^8$ s^{-1}, while maps c) and d) are calculated for $\gamma_{1,2} = 10^8$ s^{-1}.

Despite the presence of the opposite signs of v_{01} in Fig. 6(a), the distribution $N(\Delta_1, \Delta_2)$ in Fig. 6(b) is smooth. The lower bifurcation line of Fig. 6(a) is barely seen here, while the upper line is well pronounced. Remarkably, increase of Δ_2 at $\Delta_1 \approx 0$ is favorable for the comb in spite of the increasing instability threshold, see Eq. (3). The value $N_{\max} \approx 270$, which takes place at $\Delta_1 = 0, \Delta_2 \simeq 15$, is substantially larger than the zero detunings value $N(0, 0) \approx 230$. Note also that the distribution $N(\Delta_1, \Delta_2)$ in Fig. 6(b) is almost symmetric in Δ_1 despite the pronounced Δ_1 asymmetry of the excitation threshold. The soliton profiles and comb spectra are symmetric

Optics EXPRESS

within the dark-blue areas of Fig. 6(a) and similar to those presented in Fig. 3(a,b) and 3(c,d). Within the central area they are notably asymmetric and similar to the profiles of Figs. 4(a,b) and 4(c,d).

Consider next the case of equal damping constants $\gamma_{1,2} = 10^8$ s^{-1}, see Figs. 6(c,d). Here we have $v_{01}(\Delta_1, \Delta_2) = 0$ within almost the whole area. Bistable solutions with $v_{01} = \pm|v_{01}| \neq 0$ occur only within the narrow upper area separated from the rest by a corner-like bifurcation line. Dependence $N(\Delta_1, \Delta_2)$ is substantially different from that of Fig. 6(b). Remarkably high values of N, above 400, occur near the apex at $\Delta_2/\gamma_2 \simeq 2.8$; the soliton profiles and comb spectra are symmetric here. Compared to Fig. 3(a), the side bumps of the FH profile $|F(\varphi)|^2$ become as pronounced as the dip. The background soliton values are in a full agreement with the relations of Appendix A. The number of SH comb lines N_2 around $N_{\max}$ notably exceeds N_1. Smaller values of η correspond to smaller optimum values of Δ_2. This is relevant to both Figs. 6(b) and 6(d).

Now we consider the effects of frequency detunings for nonzero values of $\delta\lambda$ relevant to the left maximum of $N(\delta\lambda)$ in Figs. 5(b2) and 5(c2). The corresponding maps of $v_{01}/2\pi R$ and N for $\eta = 30$ and same two combinations of $\gamma_{1,2}$ are presented in Fig. 7. In contrast to Fig. 6, there are no regions with $v_{01} = 0$ any more, and the soliton velocity difference v_{01} is positive in the whole considered range of detunings. Another important feature is that the maximum value of N is achieved at nonzero detunings is substantially dependend on the relationship between γ_1 and γ_2. For Fig. 7(d) we have $N_{\max} \approx 430$. Note also the absence of a visible correlation between the distributions $v_{01}(\Delta_1, \Delta_2)$ and $N(\Delta_1, \Delta_2)$. The comb spectra relevant to Figs. 7(b) and 7(d) are strongly asymmetric, and the number of SH comb lines N_2 substantially exceeds N_1. Near the points of maximum of N the comb spectra $|S_l|^2$ acquire a pronounced substructure, and the soliton profiles acquire more sharp features as compared to those shown in Figs. 4(a,b). In the cases (c,d) decrease of Δ_1 below -1.4×10^8 s^{-1} leads to new bifurcations and transition to multi-soliton and quasi-random states.

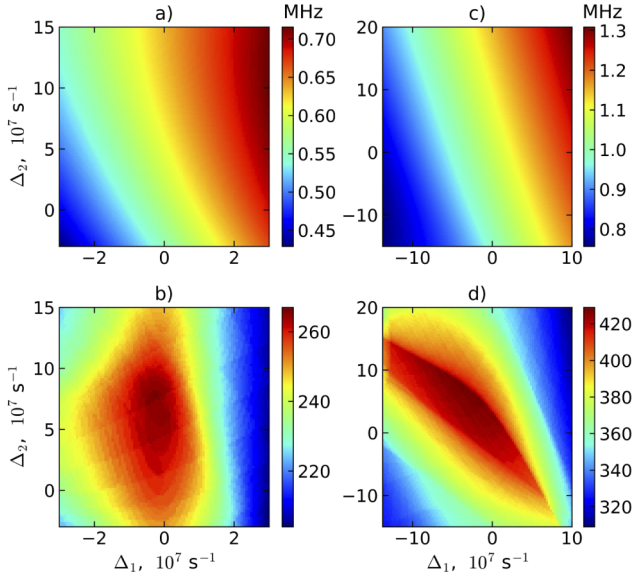

Fig. 7. Color maps of $v_{01}/2\pi R$ (the upper row) and N (the lower row) on the Δ_1, Δ_2 plane for $\eta = 30$. The left column (subfigures a and b) corresponds to $\gamma_1 = 10^7$, $\gamma_2 = 10^8$ s^{-1} and $\delta\lambda \simeq -1$ nm, and the right column (subfigures c and d) refers to $\gamma_{1,2} = 10^8$ s^{-1} and $\delta\lambda \simeq -2$ nm. The calculation procedure is the same as for Fig. 6.

Optics EXPRESS

Lastly, we consider the issue of self-starting for the soliton-comb states with nonzero detunings. In contrast to the case of zero detunings, the antiperiodic steady states considered cannot always be generated from weak noise upon an adiabatic switching on the pump power. In paricular, increasing η for $\Delta_1<0$ and $\Delta_2 = 0$, which corresponds to the low-threshold parametric excitation according to Eq. (3), results typically in steady states that can be interpreted as multi-soliton ones. Furthermore, adiabatic decrease of η starting from steady state with $\eta = 30$ ultimately ends up here with bifurcations leading to multi-soliton steady states. At the same time, increasing η for $\Delta_1>0$ and $\Delta_2 = 0$ still leads to the generation of single-soliton states. Thus, single-soliton steady states with $\Delta_{1,2} \neq 0$ are accessible either by an adiabatic increase of pump power or by adiabatic detuning changes at sufficiently large values of η. Detailed analysis of the self-starting area of our variable parameters $\eta, \delta\lambda, \gamma_{1,2}$, and $\Delta_{1,2}$ is beyond the scope of this paper.

6. Discussion

Above we have presented the results of our broad-scale study of soliton-comb generation in $\chi^{(2)}$ optical microresonators. A distinctive feature of this study is covering of a broad range of the relevant experimental parameters – the pump wavelength λ_p, the pump-strength η, FH and SH quality factors $Q_{1,2}$, and the frequency detunings $\Delta_{1,2}$ – as applied to the most common LN based resonators. It has no analogs with regard to the scale of coverage. The results obtained form numerous predictions (and also some requirements) for experiment. They strongly extend and supplement the results of [27], where the presence of accessible antiperiodic soliton-comb states was indicated for the case of constant dispersion, zero detunings, and equal FH-SH decay rates.

Our study shows that the optimization of the comb properties requires radial poling of the resonator to ensure the quasi-PM at the wavelength on demand [11,12]. The radial poling must provide a rough adjustment of the phase-matching point; the known fine-tuning means [16,41,42] have to be used for the final adjustment. A high-quality radial poling can be considered as the major technological challenge on the way of realization of broad $\chi^{(2)}$ frequency combs. Of particular interest is an adjustment to the vicinity of zero walk-off point where the coupled primary FH and SH modes possess almost the same group velocities. For LN based resonators this is relevant to SH pumping in the vicinity of $\lambda_c \simeq 1349$ nm. To the best of our knowledge, all known $\chi^{(2)}$ comb experiments correspond to very large values of the walk-off parameter, $|\alpha| \gg 1$.

Importantly, the case of SH pumping considered admits the excitation of two topologically different nonlinear states – periodic (P) and antiperiodic (A) – that correspond to pumping into the modes with even and odd azimuth numbers, respectively. These states were introduced recently in [26,27]. It turns out that within the whole actual range of the variable experimental parameters, the excitation of the A-states offers greater advantages as compared to the P-states: Typically, the A-states are not only stable, but also self-starting; they arise from noise under not very abrupt switching the pump power above the threshold value. The soliton-comb A-states form a vast family – they exist in broad ranges of η, λ_p $Q_{1,2}$, and $\Delta_{1,2}$. The known P-states [22,23] do not possess this property. The underlying reason is the presence of nonzero amplitude background $F_0 = \bar{F}$ in the case of pumping into even SH modes: As soon as this background is stable, the system can arrive to it during the nonlinear evolution. The A-states generically have no such amplitude background, $F_0 = 0$.

As follows from the above mentioned, the case of pumping into FH modes, where the primary nonlinear process is the SH generation, has to be considered separately. In this case only the P-states possessing the dual FH-SH background are present and the physical pattern of steady states (including single-soliton states) is expected to be entirely different.

As we have found, the pump wavelength area $|\delta\lambda| = |\lambda_p - \lambda_c| \lesssim 5$ nm, relevant to weak or modest walk-off and most promising for the generation of $\chi^{(2)}$ combs possesses a rich internal structure. This structure is due to an interplay between the nonlinear $\chi^{(2)}$ processes and the linear

Optics EXPRESS

effects of dispersion, temporal walk-off, and modal decay. Far enough from the λ_c point the walk-off controlled soliton-comb regimes take place, and the comb generation efficiency drops with increasing $|\delta\lambda|$. For sufficiently small values of $|\delta\lambda|$ dispersion-controlled regimes occur. The optimum values of $|\delta\lambda|$ are not attached exactly to the zero walk-off point. At zero frequency detunings they lie at $|\delta\lambda| = (1-3)$ nm depending on the values of $Q_{1,2}$; the higher Q-factors, the narrower is the near-optimum spectral distance $|\delta\lambda|$. Note also that the most promissing area of λ_p includes $\sim 10^2$ free spectral ranges; this leaves much room for the spectral adjustment via the radial poling.

Remarkably, nonzero detunings, i.e. slightly imperfect phase matching and slightly nonresonant pumping, can be favorable for the combs, as they notably increase the number of comb lines. Another remarkable prediction is the impact of the Q_2/Q_1 ratio on the soliton-comb properties. On the one hand, increase of this ratio leads to smoothing of all $\delta\lambda$ dependences, including the dependence $v_{01}(\delta\lambda)$. On the other hand, sufficiently large values of this ratio lead, in a combination with nonzero detunins, to a new nonlinear phenomenon – spontaneous breaking of spatial symmetry at $\lambda = \lambda_c$: Symmetric solitons with velocity $v_0 = v_1 = v_2$ become unstable against strong asymmetric deformations and propagation with nonzero $\pm|v_{01}|$ velocities. This phenomenon is similar to the second-order ferroelectric transitions.

All considered comb-soliton states can be accessed in experiment either via not very abrupt (slower than μs) switching on the pump power (the case of zero or small frequency detunings) or via a combination of this switching procedure with the subsequent changes of $\Delta_{1,2}$.

Note finally that the problem of existence and accessibility of multi-soliton solutions (of P and/or A type) remains open. It is beyond the scope of this study.

7. Conclusions

A number of specific predictions for the generation of soliton-related dual FH-SH frequency combs is made for lithium niobate based high-Q microresonators. The SH pumping in the close vicinity of the point of equal FH and SH group velocities, $\lambda_p \simeq 1.349\,\mu$m, implying the phase matching via proper radial poling of the resonator, is the most favorable. In doing so, the emphasis must be made on the excitation of the modes with odd azimuth number leading to the excitation of the antiperiodic soliton states. These states form a vast and experimentally accessible family within broad ranges of the experimental parameters – the pump power, the modal Q-factors, and the frequency detunings relevant to slightly imperfect phase matching and slightly nonresonant pumping. This family of dissipative dual $\chi^{(2)}$ solitons has no analogs in the literature. Among new physical effects is prediction of spontaneous symmetry breaking for the solitons similar to the second-order phase transitions.

Appendix

A. FH and SH backgrounds

According to Eqs. (1), the spatially uniform steady-state values $\bar{F}$ and $\bar{S}$ obey equations

$$-\Omega_1\bar{F} = 2\mu\bar{S}\bar{F}^*, \quad -\Omega_2\bar{S} = \mu\bar{F}^2 + \mathrm{i}h \tag{4}$$

with $\Omega_{1,2} = \Delta_{1,2} - \mathrm{i}\gamma_{1,2}$. The second equation uniquely links $\bar{S}$ to $\bar{F}^2$, while replacement $\bar{F}$ by $-\bar{F}$ in the first one changes nothing. Solutions $\pm\bar{F}$ are thus equivalent.

Consider the absolute values $|\bar{F}|$ and $|\bar{S}|$. The second one is given by $|\bar{S}| = |\Omega_1|/2\mu$. Next we express $|\bar{F}|^2$ by our super-criticality parameter $\eta = 2\mu h/\gamma_1\gamma_2$:

$$2\mu^2|\bar{F}|^2/\gamma_1\gamma_2 = \pm\sqrt{\eta^2 - z''^2} - z' \,, \tag{5}$$

Optics EXPRESS

where $z = (1+\mathrm{i}\Delta_1/\gamma_1)(1+\mathrm{i}\Delta_2/\gamma_2)$. The LHS accounts for our normalization of the FH amplitude. Only the sign + is physical in the RHS as it corresponds to a stable background. At $\Delta_{1,2} = 0$ we have $2\mu^2|\bar{F}|^2/\gamma_1\gamma_2 = \eta - 1$ and $4\mu^2|\bar{S}|^2/\gamma_1^2 = 1$.

Note that the background solution $\bar{F} = 0$, $\bar{S} = -\mathrm{i}h/\Omega_2$ is stable against small perturbations below the parametric instability threshold. Two stable branches can thus co-exist for sufficiently small values of η and large $|\Delta_{1,2}|$.

B. Equations for Fourier harmonics

Transferring in (1) to a coordinate frame moving with velocity v_1, substituting the expansions (1), and using the standard relations of Fourier analysis, we obtain:

$$\begin{aligned}\dot{F}_j + (\gamma_1 + \mathrm{i}\Delta_1 + \mathrm{i}\beta_1 j^2)F_j &= -2\mathrm{i}\mu\sum_l S_l F^*_{l-j}\\ \dot{S}_l + (\gamma_2 + \mathrm{i}\Delta_2 - \mathrm{i}\alpha l + \mathrm{i}\beta_2 l^2)S_l &= h\delta_{l,0} - \mathrm{i}\mu\sum_j F_j F_{l-j},\end{aligned} \tag{6}$$

where dot indicates differentiation in t, $\beta_{1,2} = v'_{1,2}/2R^2$, $\alpha = v_{12}/R$, and l takes values $0, \pm1, \pm2, \ldots$. This infinite set of ordinary differential equations is valid for both periodic (P) and antiperiodic (A) solutions. In the P- and A-cases, index j takes the values $0, \pm1, \pm2, \ldots$ and $\pm1/2, \pm3/2, \ldots$, respectively. Equation for S_0 includes the pumping term h, but it does not include the walk-off and dispersion terms. In equations for S_l with $l \neq 0$, the term $-\mathrm{i}\alpha l S_l$ is dominating for $\alpha \gg \gamma_2, |\beta_2|, |\Delta_2|$, and $S_l \simeq (\mu/\alpha l)\sum_j F_j F_{l-j}$ with a good accuracy. Being substituted in the first equation, it gives a small cubic nonlinear term in the equation for F_j. The walk-off case corresponds to inequality $|S_l| \ll |S_0|$, it is not favorable for the $\chi^{(2)}$ combs.

At the spectral point of equal group velocities $\lambda = \lambda_c$, where $\alpha = 0$, Eqs. (6) include only squared modal numbers j^2 and l^2. This leads to the symmetry property: If $F_j(t)$ and $S_l(t)$ is solution of set (6), then $F_{-j}(t)$ and $S_{-l}(t)$ is its solution as well. This symmetry property becomes nontrivial for $v_{01} \neq 0$.

Funding. Fraunhofer and Max Planck Cooperation Program (COSPA); Russian Foundation for Basic Research (20-02-00511).

Disclosures. The authors declare no conflicts of interest.

Data availability. Data availability Data underlying the results presented in this paper are available from the corresponding author upon reasonable request.

References

1. P. Del'Haye, A. Schliesser, O. Arcizet, T. Wilken, R. Holzwarth, and T. J. Kippenberg, "Optical frequency comb generation from a monolitic microresonator," Nature **450**(7173), 1214–1217 (2007).
2. P. Del'Haye, T. Herr, E. Gavartin, M. L. Gorodetsky, R. Holzwarth, and T. J. Kippenberg, "Octave spanning tunable frequency comb from a microresonator," Phys. Rev. Lett. **107**(6), 063901 (2011).
3. T. J. Kippenberg, R. Holzwarth, and S. A. Diddams, "Microresonator based optical frequency combs," Science **332**(6029), 555–559 (2011).
4. T. Herr, K. Hartinger, J. Riemensberger, C. Y. Wang, E. Gavartin, R. Holzwarth, M. L. Gorodetsky, and T. J. Kippenberg, "Universal formation dynamics and noise of Kerr-frequency combs in microresonators," Nat. Photonics **6**(7), 480–487 (2012).
5. T. Herr, V. Brasch, J. D. Jost, C. Y. Wang, N. M. Kondratiev, M. L. Gorodetsky, and T. J. Kippenberg, "Temporal solitons in optical microresonators," Nat. Photonics **8**(2), 145–152 (2014).
6. X. Yi, Q.-F. Yang, M.-J. Suh, and K. Vahala, "Soliton frequency comb at microwave rates in a high-Q silica microresonator," Optica **2**(12), 1078 (2015).
7. M. G. Suh and K. Vahala, "Gigahertz-repetition-rate soliton microcombs," Optica **5**(1), 65–66 (2018).
8. T. J. Kippenberg, A. L. Gaeta, M. Lipson, and M. L. Gorodetsky, "Dissipative Kerr solitons in optical microresonators," Science **361**(6402), eaan8083 (2018).
9. N. Akhmediev and A. Ankiewicz, *Dissipative Solitons, Lecture Notes in Physics* (Springer-Verlag, 2005).
10. J. U. Fürst, D. V. Strekalov, D. Elser, M. Lassen, U. L. Andersen, C. Marquardt, and G. Leuchs, "Naturally phase-matched second-harmonic generation in a whispering-gallery-mode resonator," Phys. Rev. Lett. **104**(15), 153901 (2010).

Optics EXPRESS

11. T. Beckmann, H. Linnenbank, H. Steigerwald, B. Sturman, D. Haertle, K. Buse, and I. Breunig, "Highly tunable low-threshold optical parametric oscillation in radially poled whispering gallery resonators," Phys. Rev. Lett. **106**(14), 143903 (2011).
12. M. Mohageg, D. V. Strekalov, A. A. Savchenkov, A. B. Matsko, V. S. Ilchenko, and L. Maleki, "Calligraphic poling of lithium niobate," Opt. Express **13**(9), 3408–3419 (2005).
13. A. V. Buryak, P. Di Trapani, D. V. Skryabin, and S. Trillod, "Optical solitons due to quadratic nonlinearities: from basic physics to futuristic applications," Phys. Rep. **370**(2), 63–235 (2002).
14. L. Maleki, V. S. Ilchenko, A. A. Savchenkov, and A. B. Matsko, "Crystalline whispering gallery mode resonators in optics and photonics," in *Practical Applications of Microresonators in Optics and Photonics*, A. B. Matsko, ed. (CRC, 2009).
15. I. Breunig, "Three-wave mixing in whispering gallery resonators," Laser Photonics Rev. **10**(4), 569–587 (2016).
16. D. Strekalov, Ch. Marquardt, A. Matsko, H. Schwefel, and G. Leuchs, "Nonlinear and quantum optics with whispering gallery resonators," J. Opt. **18**(12), 123002 (2016).
17. V. Ulvila, C. R. Phillips, L. Halonen, and M. Vainio, "High-power mid-infrared frequency comb from a continuous-wave-pumped bulk optical parametric oscillator," Opt. Express **22**(9), 10535–10543 (2014).
18. F. Leo, T. Hansson, I. Ricciardi, M. De Rosa, S. Coen, S. Wabnitz, and M. Erkintalo, "Walk-off-induced modulation instability, temporal pattern formation, and frequency comb generation in cavity-enhanced second-harmonic generation," Phys. Rev. Lett. **116**(3), 033901 (2016).
19. S. Mosca, I. Ricciardi, M. Parisi, P. Maddaloni, L. Santamaria, P. De Natale, and M. De Rosa, "Direct generation of optical frequency combs in $\chi^{(}2)$ nonlinear cavities," Nanophotonics **5**(2), 316–331 (2016).
20. S. Mosca, M. Parisi, I. Ricciardi, F. Leo, T. Hansson, M. Erkintalo, P. Maddaloni, P. De Natale, S. Wabnitz, and M. De Rosa, "Modulation instability induced frequency comb generation in a continuously pumped optical parametric oscillator," Phys. Rev. Lett. **121**(9), 093903 (2018).
21. T. Hannson, P. Parra-Rivas, M. Bernard, F. Leo, L. Gelens, and S. Wabnitz, "Quadratic soliton combs in doubly resonant second-harmonic generation," Opt. Lett. **43**(24), 6033–6036 (2018).
22. A. Villois and D. Skryabin, "Soliton and quasi-soliton frequency combs due to second harmonic generation in microresonators," Opt. Express **27**(5), 7098–7107 (2019).
23. A. Villois, N. Kondratiev, I. Breunig, D. N. Puzyrev, and D. V. Skryabin, "Frequency combs in a microring optical parametric oscillator," Opt. Lett. **44**(18), 4443–4446 (2019).
24. Y. He, Q-F. Yang, J. Ling, R. Luo, H. Liang, M. Li, B. Chen, H. Wang, K. Vahala, and Q. Lin, "Self-starting bi-chromatic $LiNbO_3$ soliton microcomb," Optica **6**(9), 1138–1144 (2019).
25. V. E. Lobanov, "Two-color flat-top solitons in microresonator-based optical parametric oscillators," Phys. Rev. A **102**(1), 013518 (2020).
26. E. Podivilov, S. Smirnov, I. Breunig, and B. Sturman, "Nonlinear solutions for $\chi^{(}2)$ frequency combs in optical microresonators," Phys. Rev. A **101**(2), 023815 (2020).
27. S. Smirnov, B. Sturman, E. Podivilov, and I. Breunig, "Walk-off controlled self-starting frequency combs in $\chi^{(}2)$ optical microresonators," Opt. Express **28**(12), 18006 (2020).
28. E. Podivilov, B. Sturman, and I. Breunig, "Frequency comb solutions for driven $\chi^{(}2)$ optical microresonators," J. Opt. Soc. Am. B **37**(11), 3316–3324 (2020).
29. J. Szabados, D. N. Puzyrev, Y. Minet, L. Reis, K. Buse, A. Villois, D. V. Skryabin, and I. Breunig, "Frequency comb generation via cascaded second-ordern nonlinearities in microresonators," Phys. Rev. Lett. **124**(20), 203902 (2020).
30. J. Szabados, B. Sturman, and I. Breunig, "Frequency comb generation threshold via second-harmonic excitation in $\chi^{(}2)$ optical microresonators," APL Photonics **5**(11), 116102 (2020).
31. I. Hendry, L. S. Trainor, Y. Xu, S. Coen, S. G. Murdoch, H. G. L. Schwefel, and M. Erkintalo, "Experimental observation of internally pumped parametric oscillation and quadratic comb generation in a $\chi^{(}2)$ whispering-gallery-mode microresonator," Opt. Lett. **45**(5), 1204–1207 (2020).
32. L. Chang, W. Xie, H. Shu, Q.-F. Yang, B. Shen, A. Boes, J. D. Peters, W. Jin, C. Xiang, S. Liu, G. Moille, S.-P. Yu, X. Wang, K. Srinivasan, S. B. Papp, K. Vahala, and J. E. Bowers, "Ultra-efficient frequency comb generation in AlGaAs-on-insulator microresonators," Nat. Commun. **11**(1), 1331 (2020).
33. A. W. Bruch, X. Liu, Z. Gong, J. B. Surya, M. Li, C.-L. Zou, and H. X. Tang, "Pockels soliton microcomb," Nat. Photonics **15**(1), 21–27 (2021).
34. Let the total light field be $E = S(t, \varphi)\exp(\mathrm{m_p}\varphi - \omega_p t); + F(t, \varphi)\exp(\mathrm{m_p}\varphi - \omega_p t)/2;;$ m_p is the azimuth number of the pumped SH mode. For odd m_p, 2π-periodicity of $E(\varphi)$ means antiperiodicity of $F(\varphi)$. The envelopes F, S obey generic equations, the same for even and odd m_p.
35. M. Gorodetsky and A. Fomin, "Geometrical theory of whispering-gallery modes," IEEE J. Sel. Top. Quantum Electron. **12**(1), 33–39 (2006).
36. M. L. Gorodetsky and Y. A. Demchenko, "Accurate analytical estimates of eigenfrequencies and dispersion in whipering-gallery spheroidal resonators," Proc. SPIE **8236**, 823623 (2012).
37. B. Sturman, E. Podivilov, C. S. Werner, and I. Breunig, "Vectorial perturbation theory for axisymmetric whispering gallery resonators," Phys. Rev. A **99**(1), 013810 (2019).
38. U. Schlarb and K. Betzler, "A generalized Sellmeier equation for the refractive indices of lithium niobate," Ferroelectrics **156**(1), 99–104 (1994).

Optics EXPRESS

39. D. E. Zelmon, D. L. Small, and D. Jundt, "Infrared corrected Sellmeier coefficients for congruently grown lithium niobate and 5 mol. magnesium oxide-doped lithium niobate," J. Opt. Soc. Am. B **14**(12), 3319–3322 (1997).
40. D. N. Nikogosyan, *Nonlinear Optical Crystals: A Complete Survey*, (Springer, 2005).
41. Yu. Jia, K. Hanka, K. T. Zawilski, P. G. Schunemann, K. Buse, and I. Breunig, "Continuous-wave whispering-gallery optical parametric oscillator based on $CdSiP_2$," Opt. Express **26**(8), 10833–10841 (2018).
42. J. Szabados, Ch. S. Werner, S. J. Herr, I. Breunig, and K. Buse, "Electro-optic eigenfrequency tuning of potassium tantalate-niobate microresonators," APL Photonics **5**(1), 016106 (2020).
43. B. Sturman, T. Beckmann, and I. Breunig, "Quasi-resonant and quasi-phase-matched nonlinear second-order phenomena in whispering-gallery resonators," J. Opt. Soc. Am. B **29**(11), 3087–3095 (2012).